Hua, Q., Cook, D., Fohlmeister, J., Penny, D., Bishop, P., Buckman, S. (2017): Radiocarbon Dating of a Speleothem Record of Paleoclimate for Angkor, Cambodia. - *Radiocarbon*, *59*, 6, pp. 1873—1890.

DOI: http://doi.org/10.1017/RDC.2017.115

RADIOCARBON DATING OF A SPELEOTHEM RECORD OF PALAEOCLIMATE FOR ANGKOR, CAMBODIA

Quan Hua[1], Duncan Cook[2], Jens Fohlmeister[3,4], Dan Penny[5], Paul Bishop[6], Solomon Buckman[7]

[1]Australian Nuclear Science and Technology Organisation, Locked Bag 2001, Kirrawee DC, NSW 2232, Australia. Corresponding author, email: qhx@ansto.gov.au

[2]National School of Arts, Australian Catholic University, Locked Bag 2002, Strathfield, NSW 2135, Australia

[3]Institute of Earth and Environmental Science, University of Potsdam, Karl-Liebknecht Str. 24-25, 14476 Potsdam, Germany

[4]GFZ German Research Centre for Geosciences, Section 5.2 Climate Dynamics and Landscape Evolution, Telegrafenberg Building C, D-14473 Potsdam, Germany

[5]School of Geosciences, Madsen F09, University of Sydney, NSW 2006, Australia

[6]School of Geographical and Earth Sciences, East Quad, University of Glasgow, Glasgow G12 8QQ, UK

[7]School of Earth and Environmental Sciences, University of Wollongong, NSW 2522 Australia

Keywords: Tropical speleothems, radiocarbon, chronological construction, Angkor, Southeast Asia

ABSTRACT

We report the chronological construction for the top portion of a speleothem, PC1, from southern Cambodia with the aim of reconstructing a continuous high-resolution climate record covering the fluorescence and decline of the medieval Khmer kingdom and its capital at Angkor (~9th-15th centuries AD). Earlier attempts to date PC1 by the standard U-Th method proved unsuccessful. We have therefore dated this speleothem using radiocarbon. Fifty carbonate samples along the growth axis of PC1 were collected for AMS analysis. Chronological reconstruction for PC1 was achieved using two different approaches described by Hua et al. (2012a) and Lechleitner et al. (2016a). Excellent concordance between the two age-depth models indicates that the top ~47 mm of PC1 grew during the last millennium with a growth hiatus during ~1250-1650 AD, resulting from a large change in measured ^{14}C values at 34.4-35.2 mm depth. The timing of the growth hiatus covers the period of decades-long droughts during the 14th-16th centuries AD indicated in regional climate records.

INTRODUCTION

Angkor was the capital district of the medieval Khmer kingdom in southeast (SE) Asia, flourishing from approximately the 9th to the 15th centuries AD. The emergence, expansion, and demise of Angkor have been studied intensively for many decades. While the probable significance of climate variability in ancient Cambodian society is understood, the lack of high-resolution palaeoclimate data from Cambodia has meant that a rigorous analysis of what role climate played in the fluorescence and demise of the Khmer kingdom has not been possible (Buckley et al. 2010). The Indochina Peninsula, unlike the better-known South and East Asian regions (Penny 2002), provides very few palaeoclimate data sets capable of testing hypothesised links between historic societal change and climate variability. Archaeologists and historians (eg, Lieberman 2009) have instead relied on palaeoclimate data from as far away as India and China to understand late Holocene climate in mainland SE Asia, despite the well-known complexity in the expression of the monsoon in these regions (e.g., Sinha et al. 2011). Recently, an annually resolved record of tree rings from a mountainous region of

southern Vietnam has provided detailed climatic information back to the mid-13th century AD, revealing periods of weaker summer monsoon rainfall coincident with the demise of the massive agrarian Khmer kingdom and its capital during the 15th century AD (Buckley et al. 2010). Gridded models based on these data and a network of other tree-ring records from the region (Cook et al. 2010) have been used to project the timing, extent and amplitude of drought over central Indochina. There remains, however, no comparable high-resolution data from the lowlands of Cambodia itself with which to validate these projections.

We have studied a speleothem, PC1, from southern Cambodia with the aim of reconstructing a continuous high-resolution climate record based on stable isotopic composition of stalagmite calcite, covering the entire Angkor period (circa 9th-15th centuries AD). The U-Th dating method is usually employed to build precise and reliable chronologies for speleothems (Hellstrom 2003; Cheng et al. 2008). However, a pilot study that attempted to date PC1 by the standard U-Th method was unsuccessful, resulting in age reversals due to suspected multiple sources of non-authigenic ^{230}Th. This problem is commonly encountered when dating tropical speleothems (Beck et al. 2001; Partin et al. 2007; Hua et al. 2012a). Radiocarbon can be used as an alternative method for dating of speleothems. This dating method requires knowledge of the dead carbon fraction (DCF), a radiocarbon reservoir effect for speleothems resulting from the contribution of "dead" carbon free of ^{14}C from bedrock and aged soil organic matter (SOM) above the cave system. Temporal variations in DCF have been reported by several researchers (e.g., Genty et al. 2001; Griffiths et al. 2012; Noronha et al. 2014), but if DCF variability in a speleothem is properly constrained, a reliable ^{14}C-based chronology is achievable (Genty et al. 1999; Hua 2009; Hua et al. 2012a). In an alternative approach, age-depth modelling with ^{14}C-dated stalagmites is possible without prior knowledge of DCF, but requires the assumption of a quasi-constant growth rate (Lechleitner et al. 2016a). In this paper, we use radiocarbon to generate a chronology for the top 51 mm of PC1.

MATERIAL AND METHODS

PC1 was collected in January 2007 in growth position ~280 m from the entrance of an unnamed cave on the northwest slopes of Phnom Chngauk, a limestone hill that rises 130 m above the alluvial plains northeast of Kampot in southern Cambodia (10º38'40''N, 104º16'20''E; see Fig.1). Thin, well-drained calcareous lithosols are found on the slopes above the cave, while the steeper slopes and ridge crests of the hill are largely exposed limestone characterised by a variety of subaerially formed rock-solution sculpture (karren). The Kampot region is in the coastal hinterland landward of the Gulf of Thailand and is characterised by a tropical monsoon climate with an average annual rainfall of ~1998 mm. The wet season from mid-May to October is driven by the southwest monsoon delivering moisture to the region from the Gulf of Thailand, and the dry season is from November to April, with drier and cooler air flowing over the region from the northeast monsoon. April is on average the warmest month with an average air temperature of 33ºC while the coolest temperatures are typically recorded in December and January with an average temperature of 23ºC. PC1 is a stalagmite (~490 mm in length, 5.4 kg by weight) composed of porous, white/brown calcite (Fig. 2a). Although cave drip precipitation onto the speleothem and adjacent cave floor appeared recent with precipitates being shiny and translucent, the timing of the collection of PC1 in the middle of the dry season (January) might mean that the hydrological network was inactive and no active drips were observed within the cave.

In this paper we focus on the top 51 mm of PC1. In this part of the stalagmite, two small sections at depths (distance from tip) 34.4-35.2 mm (section 1) and 47.2-49.4 mm (section 2) are observably more powdery and less dense than the surrounding calcite matrix. These sections, both with clear upper and lower boundaries, might represent distinct periods of slow growth or growth hiatuses. To better understand the growth patterns of the stalagmite through these two sections, a 40 µm-thick plate of the top ~65 mm of PC1 (Fig. 2b) was prepared for thin-section and scanning electron microscope (SEM) examination. We used standard SEM imaging on a JEOL JSM-6490LV variable pressure SEM with a 15 kV conventional tungsten filament thermionic source. This analysis was completed through the AZtecSynergy and AZtecEnergy software suites at the Electron Microscopy Centre (EMC) at the University of Wollongong. We used an Oxford Instruments 80mm2 X-Maxn SDD EDS to complete semi-quantitative

elemental analysis of spots and compositional mapping, enabling us to identify the major element concentrations of growth bands through these two sections.

The uppermost layer of ~0.2 mm thick at the tip of PC1 was degraded and peeled off from the stalagmite. A Micromill 2000 LE-ER system with a 0.5-mm tungsten carbide milling bit was used to collect carbonate powders along the growth axis of PC1 for accelerator mass spectrometry (AMS) ^{14}C analysis. PC1 was milled at 200-µm intervals from 0.2 mm to 51.2 mm depth (see Fig. 2b). In the top 39.8 mm, 3-4 mg of carbonate powder for each sample was collected. However, only ~0.5-2 mg of carbonate powder per sample was obtained for the depths of 39.8-51.2 mm due to changes in the direction of growth layers below the surface of the sampling track. A total of 50 carbonate samples were reacted with 85% H_3PO_4 on a hot block at 90°C for 1hr and the evolved CO_2 was then converted to graphite using the Fe/H_2 method (Hua et al. 2001). AMS ^{14}C measurement was carried out using the STAR Facility at ANSTO (Fink et al. 2004) with a typical analytical precision of better than 0.4% (1σ). Radiocarbon content of the stalagmite samples, after correction for machine background, procedural blank and isotopic fractionation using measured $\delta^{13}C$, is reported as percent modern carbon (pMC; Stuiver and Polach 1977).

The chronological reconstruction for PC1was performed using two different approaches. The first approach, described by Hua et al. (2012a), estimated a "maximum" range of pre-bomb DCF. To cover possible changes in DCF over a short period of time (e.g., the last ~1-2 ka), a constant DCF value with variation at double the estimated pre-bomb DCF range was used to correct the speleothem radiocarbon reservoir effect. A chronology of PC1 was built based on a series of DCF-corrected ages using the Bayesian OxCal P_sequence deposition model (Bronk Ramsey 2008). The second approach (Lechleitner et al. 2016a) reconstructed the chronology by calculating the best-fit growth rate between a sequence of PC1 ^{14}C data and a terrestrial radiocarbon calibration curve, and anchoring the estimated growth rate to a point of known age. This method does not depend on any prior knowledge or estimate of the DCF. However, it requires that speleothem DCF is stationary but not necessarily constant and stalagmite growth can be well approximated with a constant rate.

RESULTS

The AMS ^{14}C results are reported in Table 1 and illustrated in Fig. 3. The ^{14}C content is ~58 pMC at depth ~48-51 mm then abruptly increases to ~82 pMC at depth ~47 mm. The value varies around 82 pMC between ~47 and ~37 mm in depth, then slightly increases to 85 pMC at depth 35.3 mm and to ~90 pMC at depth 34.5 mm. The ^{14}C content then fluctuates around 90-91 pMC between 34.5 and 9.7 mm in depth before rising again and finally reaching a maximum value of ~103 pMC at 0.3 mm depth. In general, the ^{14}C content increases upwards in the stalagmite as expected.

Large changes in the ^{14}C content over sections 1 and 2 are observed (Fig. 3 and Table 1). For section 1 (34.4-35.2 mm depth), the values of the two samples across the upper boundary (OZT930 outside section 1 of 89.94 ± 0.28 pMC and OZU220 inside section 1 of 90.32 ± 0.29 pMC) agree well with each other within 1σ uncertainties. Similarly, there is good agreement within 1σ uncertainties for the two samples across the lower boundary (OZU221 inside section 1 of 85.33 ± 0.28 pMC and OZT931 outside section 1 of 85.07 ± 0.26 pMC). For section 2 (47.2-49.4 mm depth), good concordance within 1σ uncertainties is observed for the two samples across the upper boundary (OZT937 outside section 2 of 82.30 ± 0.35 pMC and OZU222 inside section 2 of 82.12 ± 0.33 pMC). In addition, the ^{14}C content of sample OZU223, collected at depth 48.3 mm in the middle of section 2, of 58.68 ± 0.29 pMC is slightly higher than that of sample OZT943 at depth 49.5 mm just outside section 2 of 57.29 ± 0.29 pMC as the two values do not overlap within 2σ uncertainties. These ^{14}C data might indicate that there are continuous growths across the boundaries of the two sections.

However, thin-section and SEM examination (Fig. 4) reveals that these sections are not periods of continuous growth and are actually growth hiatuses. Figs. 4a-b show a dark-coloured band of section 1 (marked as h1 in the figures), composed of organic-rich, lower density deposition that must have accumulated during years of little or no drip water and calcite deposition. SEM examination of the upper boundary of section 1confirms the dominance of dark-coloured carbon-rich material inside the section (spectrum 4) close to the end of the growth hiatus (Figs. 4c-d). In contrast, denser, light-coloured carbonate material deposited above h1 (spectrum 1) marks the cessation of the growth hiatus and most likely records a return to more humid conditions and (more)

continuous drip water flow (Figs. 4c,e). Thin-section and SEM examination of section 2 showed similar findings (data are not shown). These results do not conflict the ^{14}C data, which show good agreement across the boundaries of the two hiatus sections as discussed above, because although less abundant carbonate still occurs within these sections (see Figs. 4c-d). This implies that reliable information on speleothem growth patterns and hiatuses can only be achieved by the combination of thin-section and SEM examination and dating (e.g., ^{14}C data).

The observed pMC increases in the top 8.9 mm of PC1 (from 92 to ~103 pMC) might indicate an invasion of bomb radiocarbon (Fig. 3), which is due to atmospheric nuclear testing mostly in the late 1950s and early 1960s (Levin and Hesshaimer 2000; Hua and Barbetti 2004). The shape of the bomb curve in PC1, with two small peaks at 5.9 and 3.3 mm depth superimposed on a long-term increase in the ^{14}C content, is not commonly observed in previous work (Hodge et al. 2010; Hua et al. 2012a; Noronha et al. 2015 and references therein). There are 3 depths, which are possible to represent the onset of bomb ^{14}C in PC1: 1.3, 5.9 and 8.9 mm.

The first possibility means that the bomb radiocarbon is recorded only in top 1.3 mm of PC1 because of a fast ^{14}C increase from 93 to ~103 pMC. If this option were the case, the two pre-bomb short-term ^{14}C variations peaked at 5.9 and 3.3 mm depth (likely spanning the period ~1940-1955) would be due to DCF changes related to changes in hydrology (Fohlmeister et al. 2010; Griffiths et al. 2012; Noronha et al. 2014; Lechleitner et al. 2016b). One would therefore expect large decreases in rainfall at the study site during ~1940-1955 (relative to the previous time interval) in order to generate DCF decreases and consequently speleothem ^{14}C increases from ~92 pMC at depth 6.5-8.9 mm to ~93-94.5 pMC at depth 1.7-5.9 mm. However, rainfall data from Cambodia[1] indicate the period of ~1940-1955 is ~2-16% higher than the 1900-2012 annual average value. This together with the likely short soil/karst residence time of cave drip water

---

[1]Rainfall data were taken from the Climate Change Knowledge Portal (http://sdwebx.worldbank.org/climateportal/index.cfm?page=downscaled_data_download&menu=historical).

from the literature, which is less than 1 year (Johnson et al. 2006; Noronha et al. 2015) to no more than 3-4 years at maximum (e.g., Kluge et al. 2010), suggests that ^{14}C increases at 1.7-9.7 mm depth are not related to DCF changes. In addition, the onset of bomb ^{14}C at 1.3 mm depth requires a large reduction in the growth rate for the top 1.3 mm of PC1 (1.3mm/50 yr = 0.026 mm/yr) compared to that for the previous section of 1.7-34.4 mm depth of 0.049-0.068 mm/yr derived from the two dating approaches (Hua et al. 2012a; Lechleitner et al. 2016a) mentioned above. This substantial growth rate change is unlikely because there are no obvious changes in the texture of PC1 in the top 34.4 mm. Such evidence suggests that the placement of the onset of bomb radiocarbon at 1.3 mm depth is very unlikely.

The other 2 options with the onset of bomb radiocarbon at 5.9 and 8.9 mm depth indicate that the bomb curves in PC1 are very similar to the recently published bomb curve in an U-Th dated stalagmite (CRC-3) from southern California (McCabe-Glynn et al. 2013), which shows a small and gradual ^{14}C increase between 1955 and 1960 followed by a large and sharp rise in ^{14}C around 1990. McCabe-Glynn et al. (2013) mentioned that contribution from a large proportion of SOM with slow turnover time led to their speleothem ^{14}C record that was damped and lagged relative to the atmosphere. We ran a simple carbon cycle mixing model described in Fohlmeister et al. (2011) and Griffiths et al. (2012) to see whether the model can reproduce the PC1 bomb data. The modelled ^{14}C data fit our measured ^{14}C values for PC1 well (see Fig. A1), indicating that the onset of bomb ^{14}C at 5.9 and 8.9 mm depth are both possible. In both options, the contribution of slow SOM reservoirs to PC1 is dominant (94% of 130 year-old SOM reservoir for the 5.9 mm option and 86% of 80 year-old SOM reservoir for the 8.9 mm option). This result is similar to the finding of McCabe-Glynn et al. (2013) for stalagmite CRC-3 mentioned above.

For the 2nd option with bomb ^{14}C onset at 5.9 mm depth, the speleothem growth rate for the post-bomb is 0.118 mm/yr (5.9 mm/50 yr), which is similar to that for the previous section of PC1 (5.9-34.4 mm depth) of 0.087-0.102 mm/yr based on the two dating methods (Hua et al. 2012a; Lechleitner et al. 2016a; see discussion later). While the growth rate for the 3rd option with bomb ^{14}C onset at 8.9 mm depth is 0.178 mm/yr (8.9 mm/50 yr) for the post-bomb, which is much higher than that for the previous section of

PC1 (8.9-34.4 mm depth) of 0.092-0.127 mm/yr derived from the two dating methods (data are not shown). These estimated growth rates for the top 34.4 mm, which shows no obvious changes in the calcite texture of PC1, suggest that the onset of bomb ^{14}C at 5.9 mm depth is more likely. This, however, cannot completely rule out the 3rd option with the onset of bomb ^{14}C at 8.9 mm depth.

The radiocarbon results indicate the following patterns of growth in the top 51 mm of PC1 (Fig. 3):

- A period of growth hiatus within section 2 (47.2-49.4 mm depth),
- A period of almost constant growth rate between 47.2 and 35.2 mm depth,
- Another short period of growth hiatus within section 1 (34.4-35.2 mm depth), and
- A period of growth in the top 34.4 mm with an almost constant rate.

CHRONOLOGIES FOR PC1

Dated speleothems based on laminae counting (compared to U-Th dated speleothems) are more appropriate for the precise determination of the timing of the onset of bomb ^{14}C in speleothems due to small uncertainties associated with the counting. We revisited five relevant dated stalagmites from the Northern Hemisphere based on laminae counting that their bomb ^{14}C data were published, including two (Han-stm5b and Fau-stm14) from Genty et al. (1998) and Genty and Massault (1999), one (Gib04a) from Mattey et al. (2008), one (Obi84) from Smith et al. (2009), and one (HS4) from Noronha et al. (2015). The timing of the onset of bomb ^{14}C in these speleothems is in the range of 1955-1959 or 1957 ± 2, indicating a negligible time lag between the onset of bomb ^{14}C in speleothems and that in the atmosphere, which occurs in 1955 for the Northern Hemisphere (Hua and Barbetti 2004; Hua et al. 2013). This is because there is a fast component (e.g., root respiration and fast SOM decomposition) in the soil-to-speleothem carbon transfer system (Genty and Massault 1999), which quickly transfers contemporary ^{14}C into speleothems.

The likely onset of bomb ^{14}C in PC1 is at 5.9 mm in depth (sample OZR170; see Fig. 3 and Table 1) and its timing is 1957 ± 2 AD. This timing is necessary for both chronological modelling approaches because it indicates the depth of pre-bomb samples for the estimation of pre-bomb DCF in the first approach and serves as an anchor point in the second approach.

Atmospheric ^{14}C over tropical regions in SE Asia is a result of Northern and Southern Hemisphere air-masses mixing via the monsoon systems (Hua et al. 2004a, 2004b, 2012b; Hua and Barbetti 2007). In particular, atmospheric ^{14}C for Thailand in the Northern Hemisphere is strongly influenced by the entrainment of Southern Hemisphere air parcels during the southwest Asian monsoon, when the Inter-Tropical Convergence Zone moves northwards. Such atmospheric transport and mixing result in a regional ^{14}C offset for Thailand (with Thailand being younger than the Southern Hemisphere of 21 ± 6 yr on average for the period AD 1620-1780; Hua et al. 2004b), which neighbours our study site in southern Cambodia. We therefore used the SHCal13 calibration data (Hogg et al. 2013) with this small offset of -21 ± 6 yr for the chronological development of PC1, consistent with recent work on ^{14}C chronologies for Cambodia (Beavan et al. 2012; Hendrickson et al. 2013, 2017; Pryce et al. 2014; Leroy et al. 2015; Hall et al. 2016).

First approach – Hua et al. (2012a)'s method

Genty et al. (1999) reported paired U-Th and ^{14}C analyses for two Holocene stalagmites from Europe and first discussed the potential use of radiocarbon with average DCF over time, derived from the paired U-Th and ^{14}C samples, for dating speleothems. Hua et al. (2012a) went further to develop a method of reliable dating of young speleothems of ~1-2 ka old using radiocarbon. This method employs a constant pre-bomb DCF similar to that used by Genty et al. (1999). However, in Hua et al.'s method uncertainty associated with constant DCF value is enlarged and the relative variation in the DCF is considered large enough (see discussion later in this section) to cover possible temporal variability in DCF for a short period of time. In addition, Hua et al. (2012a) uses a dense sequence of ^{14}C samples and Bayesian statistical models (e.g., OxCal and/or Bacon;

Bronk Ramsey 2008; Blaauw and Christen 2011) to build reliable ^{14}C chronologies for young speleothems.

DCF of a speleothem sample was calculated using the following equations

$$DCF = \left(1 - \frac{A_{spel.initial}}{A_{atm.\ initial}}\right) * 100\% \quad (1)$$

where respective initial radiocarbon contents of the speleothem and the atmosphere are given by:

$$A_{spel.\ initial} = A_{spel}/e^{-\lambda t} \quad (2)$$

$$A_{atm.\ initial} = A_{atm}/e^{-\lambda t} \quad (3)$$

where $\lambda = 1/8267\ yr^{-1}$ is the decay constant of radiocarbon

From (1), (2) and (3)

$$DCF = \left(1 - \frac{A_{spel}}{A_{atm}}\right) * 100\% \quad (4)$$

where A_{spel} is measured pMC value of a speleothem sample at a given time t and A_{atm} is its associated atmospheric pMC value.

The average pre-bomb DCF value for the top portion of PC1 was determined using equation (4) with A_{spel} being the weighted mean value of the ^{14}C content of thirteen samples from 6.5 to 14.7 mm depth (see Table 1) and A_{atm} representing the weighted mean value of contemporaneous atmospheric ^{14}C. The top 5.9 mm of PC1, where the bomb radiocarbon signal is observed, covers a period of 50 yr from 1957 to 2007. If there are similar growth rates for the top 14.7 mm of PC1, the timing of sample OZT195 at 14.7 mm is ~ 1880 AD. We, however, calculated A_{atm} for a much longer time period spanning between 1800 and 1950AD (instead of 1880-1950 AD based on similar growth rates) in order to obtain a larger spread for A_{atm} and consequently a "maximum" range of estimated pre-bomb DCF for PC1. The pre-bomb DCF value was in the range of 6.6-8.0% (1σ) or 7.3 ± 0.7% (1σ) calculated from A_{spel} of 91.28 ± 0.65 pMC and A_{atm} of 98.46 ± 0.20 pMC. This estimated DCF range was very similar if different A_{atm} values spanning between 20 years (1930-1950 AD) and 200 years (1750-

1950 AD) before 1950 AD were used, confirming the robustness in our approach in estimating the "maximum" pre-bomb DCF range for PC1.

A constant pre-bomb DCF for PC1 7.3 ± 1.4% (1σ), with double the variation (i.e., twice the calculated uncertainty of 0.7%), was used for speleothem ^{14}C age correction. This approach aims to cover possible temporal DCF variability for PC1 for a short period of time (e.g., ~1000 yr in this study) in order to obtain an age-depth model for PC1 agreeing with its true ages within modelled age uncertainties. In addition, the pre-bomb DCF value for PC1 of 7.3 ± 1.4%, indicating a relative variation in this DCF of (1.4/7.3)*100% = 19.2%. In most cases (15 out of 17), this relative DCF variation is higher than those of previously published speleothem DCF over different (and mostly longer) time periods (see Table 2). This comparison indicates that variability of the pre-bomb DCF value for PC1 is large enough to cover possible temporal changes in DCF for short period of time of ~1000 years, implying reliable radiocarbon dating of PC1 based on this method.

Chronological reconstruction for PC1 was achieved using the estimated timing of the onset of bomb ^{14}C in PC1 at 5.9 mm depth of 1957 ± 2 and DCF-corrected ^{14}C ages, and the OxCal P_sequence with variable accumulation rate *k* (Bronk Ramsey and Lee 2013) taking into account growth stop for sections 1 and 2. Age-depth modelling results are shown in Figs. 5a-b with a model agreement index (A_{model}) of 154%, much higher than the accepted level of 60% (Bronk Ramsey 2008).

Second approach - Lechleitner et al. (2016a)'s method

This approach establishes a relationship between radiocarbon decay (regular decreases in the ^{14}C content with depth) and the long-term stationary speleothem growth rate, which can be expressed by the following equations:

$$\ln(A_{spel}/A_{spel.\ initial}) = -\lambda t \quad (5)$$

or

$$\ln(A_{spel}/A_{spel.\ initial}) = -\lambda * d/R \quad (6)$$

where d is depth and R is the long-term growth rate.

The radiocarbon chronology of a speleothem is built based on an anchor point of known age and an R estimated using an iterative, MATLAB-based process taking into account variations in atmospheric ^{14}C (Lechleitner et al. 2016a). Thus, this method is not dependent on any *a priori* knowledge or estimate of the DCF. In addition, variations in the DCF, which could also be large, are allowed, providing that stationarity of DCF is assumed. The DCF values will be calculated after the age-depth model is established.

We ran the MATLAB program described in Lechleitner et al. (2016a) with an anchor point (OZR170 at 5.9 mm depth) of 1957 AD and taking into account a growth hiatus for section 1. An age-depth model for the top 47.2 mm of PC1, based on this approach, is also shown in Fig. 5b.

DISCUSSION

The chronology based on the first approach indicates that the top 51 mm of PC1 grew in the past ~4300 yr with a period of growth hiatus during ~2000 BC-1050 AD at ~47-49 mm depth, and a much shorter hiatus of ~1250-1670 AD at 34.4-35.2 mm depth (Figs. 5a-b). We are particularly interested in the top ~47 mm of PC1 because it incorporates the Angkor Period (~9th-15th centuries AD) and the subsequent "Middle Period" (15th-19th centuries AD). In addition, our model assumption of a constant DCF can be met for a short time span (the last ~1000 yr) and consequently a reliable chronology for this speleothem portion can be achieved.

Excellent agreement between the two age-depth models within 1σ uncertainties is observed for the top ~47 mm of PC1 (Fig. 5b). For the younger portion (5.9-34.4 mm depth), uncertainties associated with the chronology based on the second approach are much smaller than those derived from the first approach, but the reverse is observed for older portion (35.2-47.2 mm). The reason for more precise chronology produced by the second approach for the younger portion of PC1 is the well-defined decay fit of the data. This is only possible, if DCF variations are small compared to the amount of radiocarbon lost due to decay. In contrast, the larger age uncertainty of the second

method (compared to that of the first approach) can be explained by the calibration step of the DCF-corrected radiocarbon values necessary for the older portion, in which a well-defined anchor point is missing. The bunch of resulted calibrated ages gives a large range of possibilities for the line of constant growth derived from the decay fit. Thus, the need to replace the missing anchor point this way produces larger uncertainties.

The constant DCF value used in the first approach of 7.3 ± 1.4% (1σ) is not different from the average DCF values by the second approach, which were calculated after the establishment of the age-depth relationship, of 7.3 ± 0.7% (1σ) and 7.3 ± 1.1% (1σ) for the younger and older portions, respectively. Average growth rates estimated from the two approaches are also similar. For the older portion (35.2-47.2 mm depth), average growth rates are 0.060 ± 0.022 and 0.058 ± 0.024 mm/yr derived from the first and second methods, respectively. For the younger portion (5.9-34.4 mm depth), these values are 0.102 ± 0.026 and 0.087 ± 0.010 mm/yr, respectively, which are similar to the average growth rate for the post-bomb portion (the top 5.9 mm) of 0.118 mm/yr (5.9 mm/50 yr). These results demonstrate that if speleothem growth rate and DCF do not largely change with time, good concordance between the two dating approaches can be achieved.

The age-depth models shown in Fig. 5b and the growth rates discussed above indicate that the PC1 portion of 35.2-47.2 mm depth grew during ~1050-1250 AD and the top 34.4 mm portion grew faster between ~1650 (1670 and 1630 based on the first and second approaches, respectively) and 2007 AD. These two periods of growth were interrupted by a growth hiatus within section 1 (34.4-35.2 mm depth) during ~1250-1650 AD with 1σ uncertainties of ~100 years. The duration of this growth hiatus covers the period of the decades-long droughts in the region around 1360, 1410 and 1480 AD (Fig. 6; Sinha et al. 2011), which is based on speleothem $\delta^{18}O$ records from Dandak Cave in central-eastern India (Sinha et al. 2007; Berkelhammer et al. 2010) and Wanxiang Cave in central China (Zhang et al. 2008), and the Palmer Drought Severity Index (PDSI) reconstruction from Bidoup Nui-Ba National Park (BDNP) tree rings from southern Vietnam (Buckley et al. 2010). The 14th and early 15th century droughts, punctuated by a brief "pluvial" episode at the end of the 14th/start of the 15th century, has been implicated in the demise of Angkor during the 15th century AD (Buckley et al.

2010). Although these decades-long droughts do not appear in all of the three regional climate records (e.g., the drought period centred on ~1480 AD is only observed in the Wanxiang speleothem and BDNP tree-ring records), the clear phase of growth hiatus recorded in section 1 of PC1 is best explained as reflecting reduced precipitation in southern Cambodia at this time, supporting the occurrence of multi-decadal drought across the region during the 14th-16th centuries AD. Furthermore, the PC1 stalagmite record provides the strongest evidence so far that this well-documented period of historical drought may have impacted the lowland regions of Cambodia, providing important new insights into the history of climate during the fluorescence and demise of the ancient Khmer at Angkor.

The above discussions are for the most likely option of the first appearance of bomb ^{14}C in PC1 at 5.9 mm depth (the 2nd option). The 3rd option with the onset of bomb ^{14}C at 8.9 mm depth is considered as less likely due to large difference in PC1 growth rate between the top 8.9 mm and 8.9-34.4 mm depth as mentioned previously. However, if the 3rd option is correct, the chronology for the top ~47 mm of PC1 shown in Fig. 5b is shifted by ~40 years on average to the younger timescale (45 and 38 years for the first and second methods, respectively). This age shift is less than 1σ uncertainties associated with the modelled ages (in most cases) and results in the timing of the growth stop within section 1 of ~1290-1690 AD with 1σ uncertainties of ~100 years. This timing still covers the regional decades-long droughts during the 14th-16th centuries AD and consequently does not change the above discussion on regional climate.

CONCLUSION

The top portion of a tropical stalagmite, PC1, from southern Cambodia has been dated by radiocarbon using the two methods reported by Hua et al. (2012a) and Lechleitner et al. (2016a). The results show excellent agreement between the two age-depth models, indicating that the top ~47 mm of PC1 grew during the last Millennium. Our radiocarbon-based chronology for the difficult-to-date speleothem, PC1, shows a clear period of growth hiatus, that is best explained by prolonged drought conditions over the

Indochina Peninsula during the 14th -16th centuries AD, confirming previous findings of drought identified in regional proxy records.

ACKNOWLEGEMENTS

AMS ^{14}C measurements were supported by AINSE grant (13/021) and ANSTO's Environment Theme. We acknowledge the financial support from the Australian Government for the Centre for Accelerator Science at ANSTO through the National Collaborative Research Infrastructure Strategy (NCRIS). We also acknowledge funding and support from the UK Arts and Humanities Research Council (Award 119196) and the Scottish Universities Environmental Research Centre (SUERC). J.F. acknowledges funding by the German Science Foundation (grants: FO809/2-1 and FO809/4-1). We thank S. Hankin for the preparation of Fig. 1 and B. Buckley for the generous provision of tabulated tree-ring-based PDSI data shown in Fig. 6. We also thank W. Beck, A. Noronha and an anonymous reviewer for their useful comments, which improved the manuscript.

REFERENCES

Bajo P, Borsato A, Drysdale R, Hua Q, Frisia S, Zanchetta G, Hellstrom J, Woodhead J. 2017. Stalagmite carbon isotopes and dead carbon proportion (DCP) in a closed system situation: An interplay between sulphuric and carbonic acid dissolution. Geochimica et Cosmochimica Acta 210: 208-227.

Beavan N, Halcrow S, McFadgen B, Hamilton D, Buckley B, Sokha T, Shewan L, Sokha O, Fallon S, Miksic J, Armstrong R, O'Reilly D, Domett K, Chhem KR. 2012. Radiocarbon dates from jar and coffin burials of the Cardamom Mountains reveal a previously unrecorded mortuary ritual in Cambodia's late- to post-Angkor period (15th-17th centuries AD). Radiocarbon 54: 1-22.

Beck JW, Richards DA, Edwards RL, Silverman BW, Smart PL, Donahue DJ, Hererra-Osterheld S, Burr GS, Calsoyas L, Jull AJT, Biddulph D. 2001. Extremely large

variations of atmospheric ^{14}C concentration during the last glacial period. Science 292: 2453-2458.

Berkelhammer M, Sinha A, Mudelsee M, Cheng H, R. Edwards RL, Cannariato K. 2010. Persistent multidecadal power of the Indian Summer Monsoon. Earth and Planetary Science Letters 290:166-172.

Blaauw M, Christen JA. 2011. Flexible paleoclimate age-depth models using an autoregressive gamma process. Bayesian Analysis 6: 457-474.

Bronk Ramsey C. 2008. Deposition models for chronological records. Quaternary Science Reviews 27: 42-60.

Bronk Ramsey C, Lee S. 2013. Recent and planned developments of the program OxCal. Radiocarbon 55: 720-730.

Buckley, BM, Anchukaitis KJ, Penny D, Fletcher R, Cook ER, Sano M, Le CN, Wichienkeeo A, Ton That M, Truong MH. 2010. Climate as a contributing factor in the demise of Angkor, Cambodia. The Proceedings of National Academy of Sciences 107: 6748-6752.

Cheng H, Edwards RL, Shen CC,Woodhead J, Hellstrom J,Wang YJ, Kong XG, Wang XF. 2008. A new generation of Th-230 dating techniques: tests of precision and accuracy. Geochimica et Cosmochimica Acta 72: A157-A167.

Cook ER, Anchukaitis KJ, Buckley BM, D'Arrigo RD, Jacoby GC, Wright WE. 2010. Asian monsoon failure and megadrought during the last millennium. Science 328: 486-489.

Fink D, Hotchkis M, Hua Q, Jacobsen G, Smith AM, Zoppi U, Child D, Mifsud C, van der Gaast H, Williams A, Williams M. 2004. The ANTARES AMS Facility at ANSTO. Nuclear Instruments and Methods in Physics Research B 223-224: 109-115.

Fohlmeister J, Schröder-Ritzrau A, Spötl C, Frisia S, Miorandi R, Kromer B, Mangini A. 2010. The influences of hydrology on the radiogenic and stable carbon isotope composition of cave drip water, Grotta Di Ernesto (Italy). Radiocarbon 52: 1529-1544.

Fohlmeister J, Kromer B, Mangini A. 2011. The influence of soil organic matter age spectrum on the reconstruction of atmospheric ^{14}C levels via stalagmites. Radiocarbon 53: 99-115.

Genty D, Massault M. 1999. Carbon transfer dynamics from bomb-^{14}C and $\delta^{13}C$ time series of a laminated stalagmite from SW France - Modelling and comparison with other stalagmite records. Geochimica et Cosmochimica Acta 63: 1537-1548.

Genty D, Massault M, Gilmour M, Baker A, Verheyden S, Kepens E. 1999. Calculation of past dead carbon proportion and variability by the comparison of AMS ^{14}C and TIMS U/Th ages on two Holocene stalagmites. Radiocarbon 41: 251-270.

Genty D, Baker A, Massault M, Proctor C, Gilmour M, Pons-Branchu E, Hamelin B. 2001. Dead carbon in stalagmites: carbonate bedrock paleodissolution vs. ageing of soil organic matter: implications for ^{13}C variations in speleothems. Geochimica et Cosmochimica Acta 65: 3443-3457.

Griffiths ML, Fohlmeister J, Drysdale RN, Hua Q, Johnson KR, Hellstrom JC, Gagan MK, Zhao J-x. 2012. Hydrological control on the dead-carbon content of a tropical Holocene speleothem. Quaternary Geochronology 14: 81-93.

Hall T, Penny D, Hendrickson M, Cooke C, Hua Q. 2016. Iron and Fire: Geoarchaeological history of a Khmer peripheral center during the decline of the Angkorian Empire, Cambodia. Journal of Archaeological Science: Reports 6: 53-63.

Hellstrom J. 2003. Rapid and accurate U/Th dating using parallel ion-counting multicollector ICP-MS. Journal of Analytical Atomic Spectrometry 18: 1346-1351.

Hendrickson M, Hua Q, Pryce TO. 2013. Using in-slag charcoals as an indicator of "terminal" iron production within the Angkorian period (10th-13th centuries AD) center of Preah Khan of Kompong Svay, Cambodia. Radiocarbon 55: 31-47.

Hendrickson M, Leroy S, Hua Q, Kaseka P, Vuthy V. 2017. Smelting in the shadow of the Iron Mountain: Preliminary field investigation of the industrial landscape around Phnom Dek, Cambodia (9th to 20th centuries CE). Asian Perspectives 56: 55-91.

Hoffmann DL, Beck JW, Richards DA, Smart PL, Singarayer JS, Ketchmark T, Hawkesworth CJ. 2010. Towards radiocarbon calibration beyond 28 ka using speleothems from the Bahamas. Earth and Planetary Science Letters 289: 1-10.

Hogg AG, Hua Q, Blackwell PG, Niu M, Buck CE, Guilderson TP, Heaton TJ, Palmer JG, Reimer PJ, Reimer RW, Turney CSM, Zimmerman SRH. 2013. SHCal13 Southern Hemisphere calibration, 0-50,000 cal yr BP. Radiocarbon 55: 1889-1903.

Hodge E, McDonald J, Fischer M, Redwood D, Hua Q, Levchenko V, Waring C, Drysdale R, Fink D. 2011. Using the ^{14}C bomb pulse to date young speleothems. Radiocarbon 53: 345-357.

Hua Q. 2009. Radiocarbon: A chronological tool for the recent past. Quaternary Geochronology 4: 378-390.

Hua Q, Barbetti M. 2004. Review of tropospheric bomb radiocarbon data for carbon cycle modelling and age calibration purposes. Radiocarbon 46: 1273-1298.

Hua Q, Barbetti M. 2007. Influence of atmospheric circulation on regional $^{14}CO_2$ differences. Journal of Geophysical Research 112: D19102.

Hua Q, Jacobsen GE, Zoppi U, Lawson EM, Williams AA, Smith AM, McGann MJ. 2001. Progress in radiocarbon target preparation at the ANTARES AMS Centre. Radiocarbon 43: 275-282.

Hua Q, Barbetti M, Zoppi U. 2004a. Radiocarbon in annual tree rings from Thailand during the prebomb period, AD 1938-1954. Radiocarbon 46: 925-932.

Hua Q, Barbetti M, Zoppi U, Fink D, Watanasak M, Jacobsen GE. 2004b. Radiocarbon in tropical tree rings during the Little Ice Age. Nuclear Instruments and Methods in Physics Research B 223-224: 489-494.

Hua Q, McDonald J, Redwood D, Drysdale R, Lee S, Fallon S, Hellstrom J. 2012a. Robust chronological reconstruction for young speleothems using radiocarbon. Quaternary Geochronology 14: 67-80.

Hua Q, Barbetti M, Levchenko VA, D'Arrigo RD, Buckley BM, Smith AM. 2012b. Monsoonal influence on Southern Hemisphere $^{14}CO_2$. Geophysical Research Letters 39: L19806.

Hua Q, Barbetti M, Rakowski AZ. 2013. Atmospheric radiocarbon for the period 1950-2010. Radiocarbon 55: 2059-2072.

Johnson KR, Hu C, Belshaw N, Henderson G. 2006. Seasonal trace-element and stable-isotope variations in a Chinese speleothem: the potential for high resolution paleomonsoon reconstruction. Earth and Planetary Science Letters 244: 394-407.

Kluge T, Riechelmann DFC, Wieser M, Spötl C, Sültenfuß J, Schröder-Ritzrau A, Niggemann S, Aeschbach-Hertig W. 2010. Dating cave drip water by tritium. Journal of Hydrology 394: 396-406.

Lechleitner FA, Fohlmeister J, McIntyre C, Baldini LM, Jamieson RA, Hercman H, Gasiorowski M, Pawlak J, Stefaniak K, Socha P, Eglinton TI, Baldini JUL. 2016a. A novel approach for construction of radiocarbon-based chronologies for speleothems. Quaternary Geochronology 35: 54-66.

Lechleitner FA, Baldini JUL, Breitenbach SFM, Fohlmeister J, McIntyre C, Goswami B, Jamieson RA, van der Voort TS, Prufer K, Marwan N, Culleton BJ, Kennett DJ, Asmerom Y, Polyak V, Eglinton TI. 2016b. Hydrological and climatological controls on radiocarbon concentrations in a tropical stalagmite. Geochimica et Cosmochimica Acta 194: 233-252.

Leroy S, Hendrickson M, Delque-Kolic E, Vega E, Dillmann P. 2015. First direct dating for the construction and modification of the Baphuon Temple Mountain in Angkor, Cambodia. PloS ONE 10(11): e0141052.

Levin I, Hesshaimer V. 2000. Radiocarbon – A unique tracer of global carbon cycle dynamics. Radiocarbon 42: 69-80.

Lieberman, V., 2009. Strange Parallels: Volume 2, Mainland Mirrors: Europe, Japan, China, South Asia, and the Islands: Southeast Asia in Global Context, C. 800-1830 (Vol. 2). Cambridge University Press.

Mattey D, Lowry D, Duffet J, Fisher R, Hodge E, Frisia S. 2008. A 53 year seasonally resolved oxygen and carbon isotope record from a modern Gibraltar speleothem: reconstructed drip water and relationship to local precipitation. Earth and Planetary Science Letters 269: 80-95.

McCabe-Glynn S, Johnson KR, Strong C, Berkelhammer M, Sinha A, Cheng H, Edwards RL. 2013. Variable North Pacific influence on drought in southwestern North America since AD 854. Nature Geoscience 6: 617-621.

Noronha AL, Johnson KR, Hu C, Ruan J, Southon JR, Ferguson JE. 2014. Assessing influences on speleothem dead carbon variability over the Holocene: Implications for speleothem-based radiocarbon calibration. Earth and Planetary Science Letters 394: 20-29.

Noronha AL, Johnson KR, Southon JR, Hu C, Ruan J, McCabe-Glynn S. 2015. Radiocarbon evidence for decomposition of aged organic matter in the vadose zone as the main source of speleothem carbon. Quaternary Science Reviews 127: 37-47.

Oster JL, Montañez IP, Guilderson TP, Sharp WD, Banner JL. 2010. Modeling speleothem $\delta^{13}C$ variability in a central Sierra Nevada cave using ^{14}C and $^{87}Sr/^{86}Sr$. Geochimica et Cosmochimica Acta 74: 5228-5242.

Partin J, Cobb K, Adkins J, Clark B, Fernandez D. 2007. Millennial-scale trends in west Pacific warm pool hydrology since the Last Glacial Maximum. Nature 449: 452-455.

Penny D. 2012. China and Southeast Asia. In: Metcalfe SE, Nash DJ, editors. *Quaternary Environmental Change in the Tropics*. Wiley- Blackwell Publishing, Oxford. p. 207-235.

Pryce TO, Hendrickson M, Phon K, Chan S, Charlton MF, Leroy S, Dillmann P, Hua, Q. 2014. The Iron Kuay of Cambodia: Tracing the role of peripheral populations in Angkorian to Colonial Cambodia via a 1200 year old industrial landscape. Journal of Archaeological Science 47: 142-163.

Rudzka D, McDermott F, Baldini LM, Fleitmann D, Moreno A, Stoll H. 2011. The coupled $\delta^{13}C$-radiocarbon systematics of three Late Glacial/early Holocene

speleothems; insights into soil and cave processes at climatic transitions. Geochimica et Cosmochimica Acta 75: 4321-4339.

Sinha A, Cannariato KG, Stott LD, Cheng H, Edwards RL, Yadava MG, Ramesh R, Singh IB. 2007. A 900-year (600 to 1500 AD) record of the Indian summer monsoon precipitation from the core monsoon zone of India. Geophysical Research Letters 34: L16707.

Sinha A, Stott L, Berkelhammer M, Cheng H, Edwards RL, Buckley B, Aldenderfer M, Mudelsee M. 2011. A global context for megadroughts in monsoon Asia during the past millennium. Quaternary Science Reviews 30: 47-62.

Smith CL, Fairchild IJ, Spötl C, Frisia S, Borsato A, Moreton SG, Wynn PM. 2009. Chronology building using objective identification of annual signals in trace element profiles of stalagmites. Quaternary Geochronology 4:11-21.

Southon J, Noronha AL, Cheng H, Edwards RL, Wang Y. 2012. A high-resolution record of atmospheric ^{14}C based on Hulu Cave speleothem H82. Quaternary Science Reviews 33: 32-41.

Stuiver M, Polach HA. 1977. Reporting of ^{14}C data. Radiocarbon 19: 353-363.

Zhang P, Cheng H, Edwards RL, Chen F, Wang Y, Yang X, Liu J, Tan M, Wang X, Liu J, An C, Dai Z, Zhou J, Zhang D, Jia J, Jin L, Johnson KR. 2008. A test of climate, sun, and culture relationships from an 1810-year Chinese cave record. Science 322: 940-942.

Figure Captions

Figure 1 – Map of Cambodia in SE Asia showing the locations of our study site in Phnom Chngauk and Angkor.

Figure 2 – Photos of PC1 stalagmite **(a)**, and its top portion **(b)** showing micromilled trench for radiocarbon samples and thin section used for SEM examination. h1 and h2 represent section 1 and 2 discussed in the text, respectively.

Figure 3 - pMC values of samples taken from PC1. The inset diagram depicts ^{14}C content for the top ~34 mm of PC1 showing the invasion of bomb radiocarbon in the top 10.3 mm of the stalagmite. The grey shadings represent the speleothem sections of slow growth: 34.4-35.2 mm (section 1) and 47.2-49.4 mm (section 2).

Figure 4 – Thin-section and SEM examination of the top portion of PC1. **(a)** Thin section of the top ~65 mm of PC1 with h1 and h2 representing sections 1 and 2, respectively. Three bright, white regions, located below the h2 hiatus surface, are holes in the specimen from previous sample drilling, which are seen black in Fig. 2b. **(b)** A close-up image of section 1. **(c)** SEM image of the upper boundary of section 1. **(d)** and **(e)** Results of SEM semi-quantitative elemental analysis of spots inside (spectrum 4) and outside (spectrum 1) section 1, respectively.

Figure 5 – Age-depth models for **(a)** the top 51 mm of PC1 based on Hua et al. (2012a)'s approach and **(b)** the top ~47 mm of PC1 derived from Hua et al. (2012a)'s approach (black lines) and Lechleitner et al. (2016a)'s approach (grey lines). For both age-depth models, 1σ age ranges are shown.

Figure 6 – Regional palaeoclimate records of medieval drought during 1250-1650 AD. Top panel - Dandak Cave $\delta^{18}O$ record (solid line) from central-eastern India (Sinha et al. 2007; Berkelhammer et al. 2010) and speleothem $\delta^{18}O$ record from Wanxiang Cave (dashed line) in central China (Zhang et al. 2008). Bottom panel - PDSI reconstruction based on BDNP tree rings from southern Vietnam (Buckley et al. 2010). Thin and thick lines depict raw and 15 yr moving average values. Grey shadings depict regional decades-long droughts defined by Sinha et al. (2011).

Table 1 – Radiocarbon results

Table 2 - Previously published speleothem DCF values and their temporal variations

APPENDIX

Modelling the carbon transfer dynamics

One option to check the reliability for the choice of the onset of bomb radiocarbon in the stalagmite is to check if a certain age spectrum of SOM is able to explain the observed shape of the stalagmite data. For this purpose, the model of Fohlmeister et al. (2011) was used. This box-model assumes that SOM consists of three pools of different age accounting for six unknown parameters. Each pool contributes a certain portion to the total respired soil gas CO_2, which is dissolved by infiltrating water. In addition, a seventh parameter is included, representing the carbonate contribution of the host rock, which is responsible for a dilution in radiocarbon. By a random variation of these parameters it is tried to fit the measured stalagmite radiocarbon data best.

For the age-depth relationship of PC1, we assumed that the tip of the stalagmite refers to the time of removal of the speleothem (2007 AD) and that the first radiocarbon sample with bomb imprint (either 5.9 mm (2nd option) or 8.9 mm (3rd option) depth) refers to 1957 AD. The calendar ages for the samples in between the two tie points and for a short period prior to the onset of bomb ^{14}C were derived by linear interpolation. The best parameter set for both options of a possible first appearance of bomb ^{14}C, out of 100,000 simulations each, is presented together with the fit (Fig. A1).

Figure A1 – Results of the simple carbon cycle mixing model described in Fohlmeister et al. (2011) for **(a)** the 2nd option for the onset of bomb ^{14}C in PC1 at 5.9 mm depth and **(b)** the 3rd option for the onset of bomb ^{14}C in PC1 at 8.9 mm depth. Black dots are measured ^{14}C data for PC1. Solid and dashed lines are atmospheric ^{14}C and modelled speleothem ^{14}C data, respectively.

Table 1 – Radiocarbon results

Lab ID	Sample ID	Depth (mm)	$A_{spel.} \pm 1\sigma$ (pMC)
OZS157	PC1Ac-1	0.3	102.67 ± 0.62
OZS158	PC1Ac-2	0.5	97.74 ± 0.37
OZT193	PC1Ac-4	0.9	95.29 ± 0.27
OZT194	PC1Ac-6	1.3	94.90 ± 0.26
OZR164	PC1Ac-8	1.7	93.00 ± 0.41
OZR165	PC1Ac-13	2.7	93.64 ± 0.41
OZS161	PC1Ac-16	3.3	94.54 ± 0.34
OZR166	PC1Ac-18	3.7	93.72 ± 0.40
OZR167	PC1Ac-23	4.7	92.55 ± 0.38
OZR168	PC1Ac-25	5.1	93.49 ± 0.32
OZR169	PC1Ac-27	5.5	93.76 ± 0.41
OZR170	PC1Ac-29	5.9	94.22 ± 0.42
OZS163	PC1Ac-32	6.5	91.83 ± 0.35
OZR171	PC1Ac-34	6.9	92.26 ± 0.45
OZS165	PC1Ac-38	7.7	92.21 ± 0.33
OZS166	PC1Ac-41	8.3	92.23 ± 0.31
OZR172	PC1Ac-44	8.9	92.00 ± 0.43
OZS167	PC1Ac-48	9.7	91.27 ± 0.31
OZS169	PC1Ac-51	10.3	91.10 ± 0.28
OZR173	PC1Ac-54	10.9	91.10 ± 0.39
OZS170	PC1Ac-57	11.5	91.06 ± 0.31
OZS171	PC1Ac-60	12.1	90.64 ± 0.30
OZS159	PC1Ac-2b2	12.7	90.53 ± 0.32
OZS160	PC1Ac-5b2	13.3	91.10 ± 0.34
OZT195	PC1Ac-12b2	14.7	90.50 ± 0.29
OZS162	PC1Ac-20b2	16.3	90.84 ± 0.33
OZT196	PC1Ac-27b2	17.7	90.33 ± 0.30
OZS164	PC1Ac-35b2	19.3	90.07 ± 0.32
OZT197	PC1Ac-42b2	20.7	89.91 ± 0.32
OZS168	PC1Ac-50b2	22.3	90.28 ± 0.31
OZS172	PC1Ac-65b2	25.3	90.75 ± 0.29
OZT935	PC1Ac-76b2	27.5	89.87 ± 0.31
OZT927	PC1Ac-2b3	29.5	90.94 ± 0.26
OZT928	PC1Ac-13b3	31.7	89.50 ± 0.29
OZT929	PC1Ac-25b3	34.1	90.36 ± 0.30
OZT930	PC1Ac-26b3	34.3	89.94 ± 0.28
OZU220*	PC1Ac-27b3	34.5	90.32 ± 0.29
OZU221*	PC1Ac-30b3	35.1	85.33 ± 0.28
OZT931	PC1Ac-31b3	35.3	85.07 ± 0.26
OZT932	PC1Ac-41b3	37.3	82.69 ± 0.24
OZT933	PC1Ac-50b3	39.1	81.70 ± 0.25
OZT934	PC1Ac-60b3	41.1	81.13 ± 0.35
OZT936	PC1Ac-70b3	43.1	81.63 ± 0.31
OZT938	PC1Ac-80b3	45.1	82.52 ± 0.30
OZT939	PC1Ac-89b3	46.9	82.62 ± 0.35
OZT937	PC1Ac-90b3	47.1	82.30 ± 0.35
OZU222*	PC1Ac-91b3	47.3	82.12 ± 0.33

OZU223*	PC1Ac-96b3	48.3	58.68 ± 0.29
OZT940	PC1Ac-102b3	49.5	57.29 ± 0.29
OZT941	PC1Ac-110b3	51.1	57.77 ± 0.27

Note: ***-** Samples were taken inside the two speleothem sections of growth hiatus.

Table 2 – Previously published speleothem DCF values and their temporal variations

Sample	Location	DCF ± 1σ (%)	Relative variation in DCF (%)	Speleothem age	References
Fau-stm14	La Faurie (Dordogne, SW-France)	7.0 ± 0.9 (n = 11)	12.9	Pre-bomb period	Genty and Massault (1999)
Vil-stm1	Villars (SW- France)	9.4 ± 1.5 (n = 6)	16.0	3.07 – 0 ka	Genty et al. (1999, 2001)
Han-stm1	Han-sur-Lesse (Belgium)	17.5 ± 1.5 (n = 10)	8.6	11 – 4.8 ka	Genty et al. (1999, 2001)
SU-96-7	UHT, Sutherland (Scotland)	36.7 ± 1.0 (n = 10)	2.7	0.95 – 0 ka	Genty et al. (2001)
SU2	UHT, Sutherland (Scotland)	33.6 ± 4.2 (n = 4)	12.5	2.6 – 1.0 ka	Genty et al. (2001)
SU-96-1	UHT, Sutherland (Scotland)	24.5 ± 2.9 (n = 7)	11.8	3.8 – 2.0 ka	Genty et al. (2001)
Sal-stm1	Aven de la Salamandre (Gard, France)	5.3 ± 3.0 (n = 5)	56.6	6.6 – 0.1 ka	Genty et al. (2001)
GB89-24-1	Sagittarius Blue Hole (The Bahamas)	16.5 ± 2.35 (n = 68)	14.2	16 – 11 ka	Beck et al. (2001)
GB89-25-3	Sagittarius Blue Hole (The Bahamas)	22.7 ± 3.0 (n = 142)	13.2	15 – 11 ka	Hoffmann et al. (2010)
MC3	Moaning, N. California (USA)	11.0 ± 2.6 (n = 10)	23.6	10.6 – 8.8 ka	Oster et al. (2010)
GAR-01	La Garma (N. Spain)	6.5 ± 0.9 (n = 6)	13.8	11.3 – 10.2 ka	Rudzka et al. (2011)
So-1	Sofular (Turkey)	10.1 ± 1.0 (n = 4)	9.9	11.5 – 10.2 ka	Rudzka et al. (2011)
LR06B1	Flores (Indonesia)	17.2 ± 0.9 (n = 15)	5.2	2.8 – 2.4 ka	Griffiths et al. (2012)
H82	Tang Shan (China)	5.6 ± 0.7 (n = 66)	12.5	14 – 10.7 ka	Southon et al. (2012)
HS4	Hubei (China)	10.3 ± 1.5 (n = 84)	14.6	9.6 – 0.5 ka	Noronha et al. (2014)
YOK-I	Toledo (Belize)	12.8 ± 1.6 (n = 268)	12.5	AD 555 – 1952	Lechleitner et al. (2016b)
CC26	Corchia Cave (Italy)	60.1 ± 5.5 (n = 53)	9.2	12.4 – 0 ka	Bajo et al. (2017)

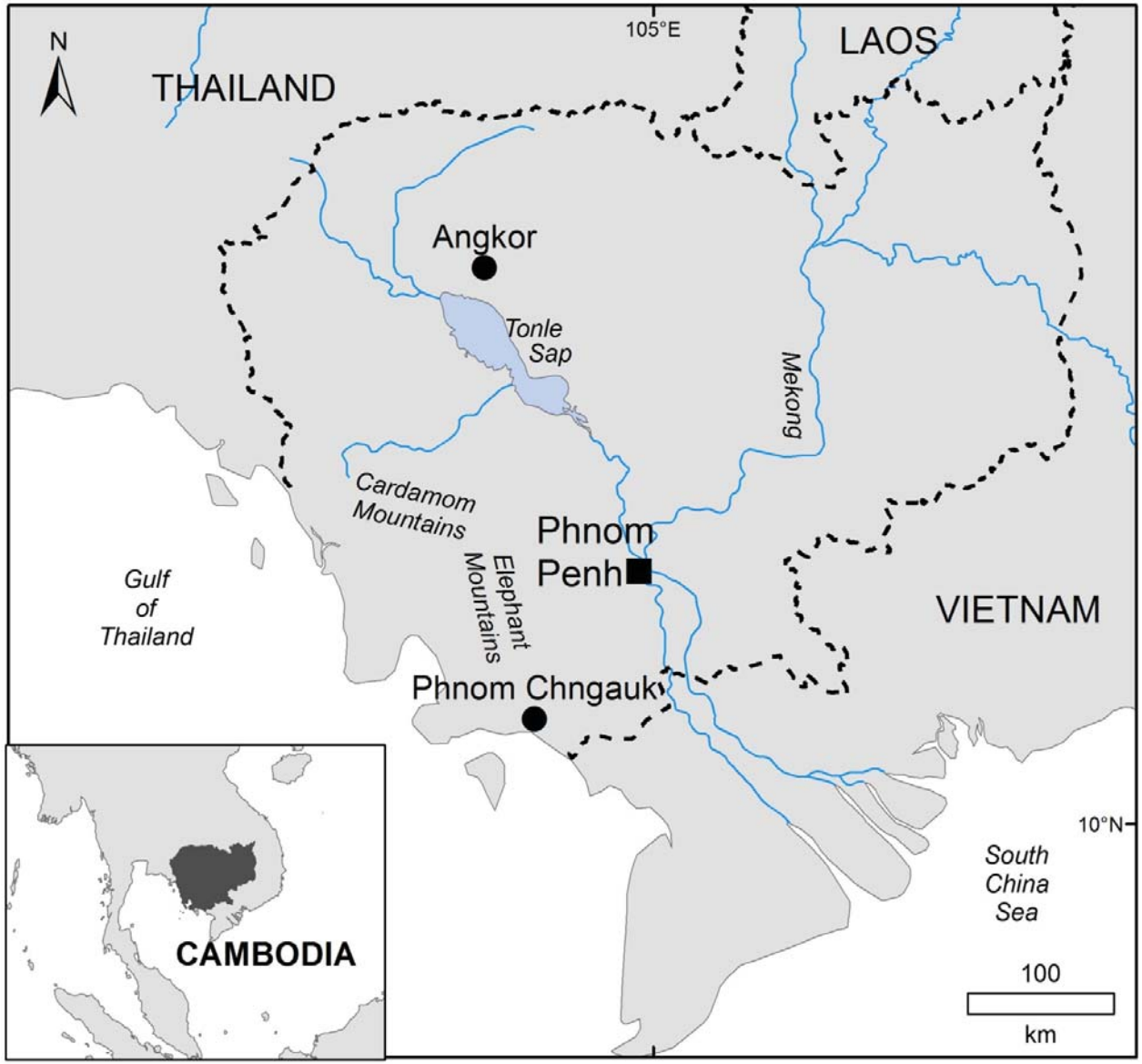
N
THAILAND
105°E
LAOS
Angkor
Tonle
Sap
Mekong
Cardamom
Mountains
Phnom
Penh
Elephant
Mountains
Gulf
of
Thailand
VIETNAM
Phnom Chngauk
10°N
South
China
Sea
100
km
CAMBODIA

Fig. 1

Fig. 2a

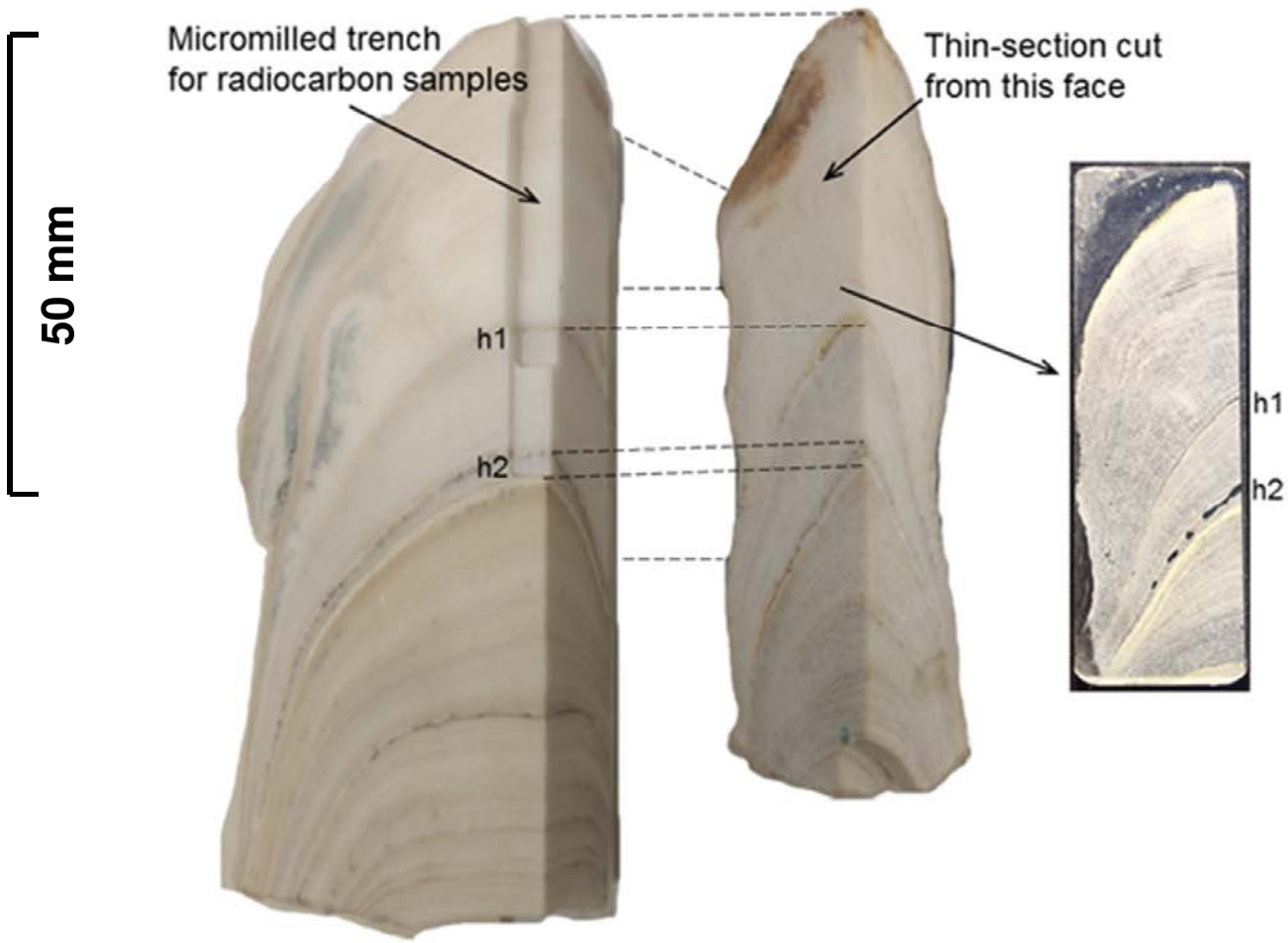
Micromilled trench
for radiocarbon samples
Thin-section cut
from this face
50 mm
h1
h2
h1
h2

Fig. 2b

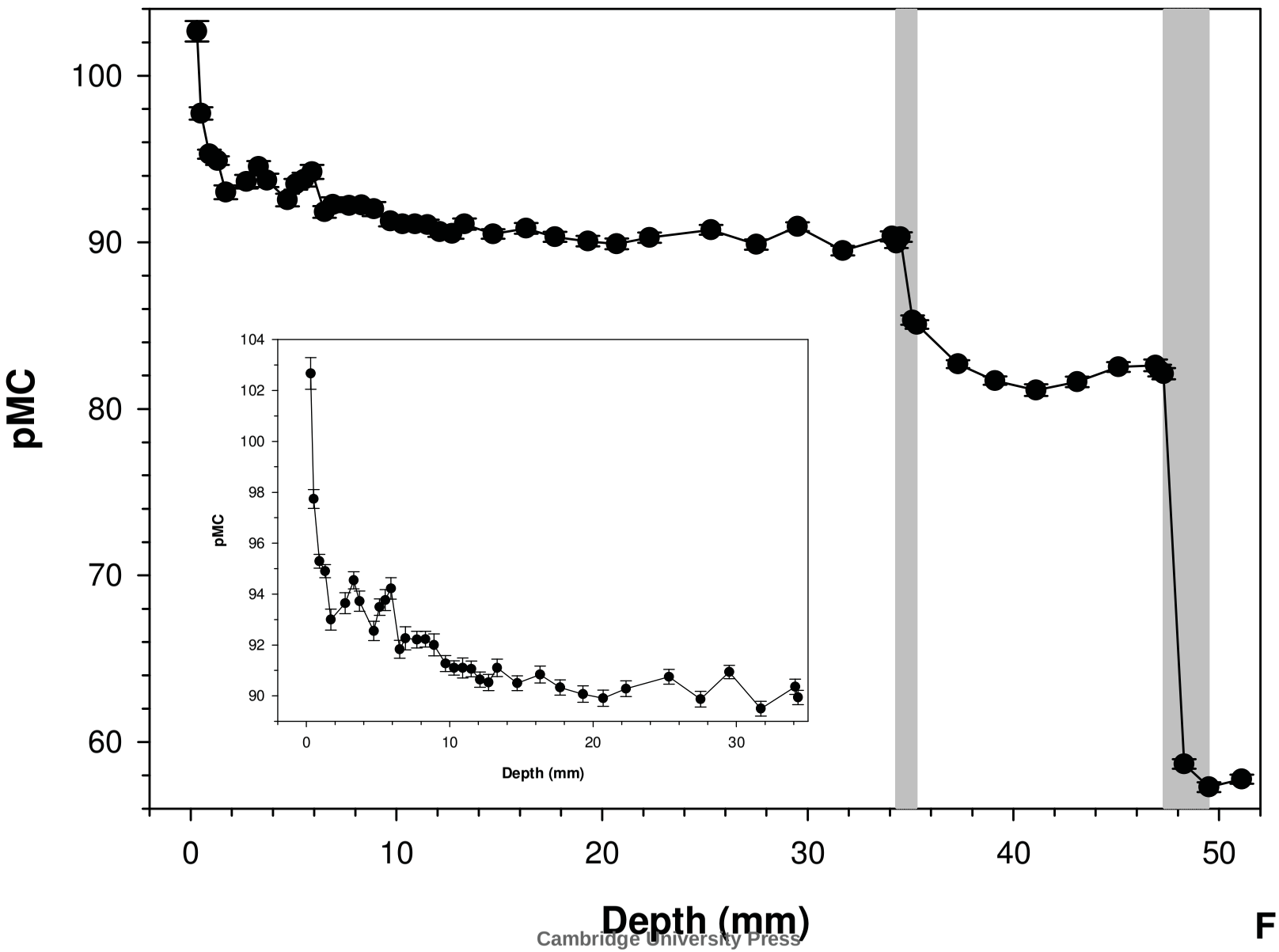

Fig. 3

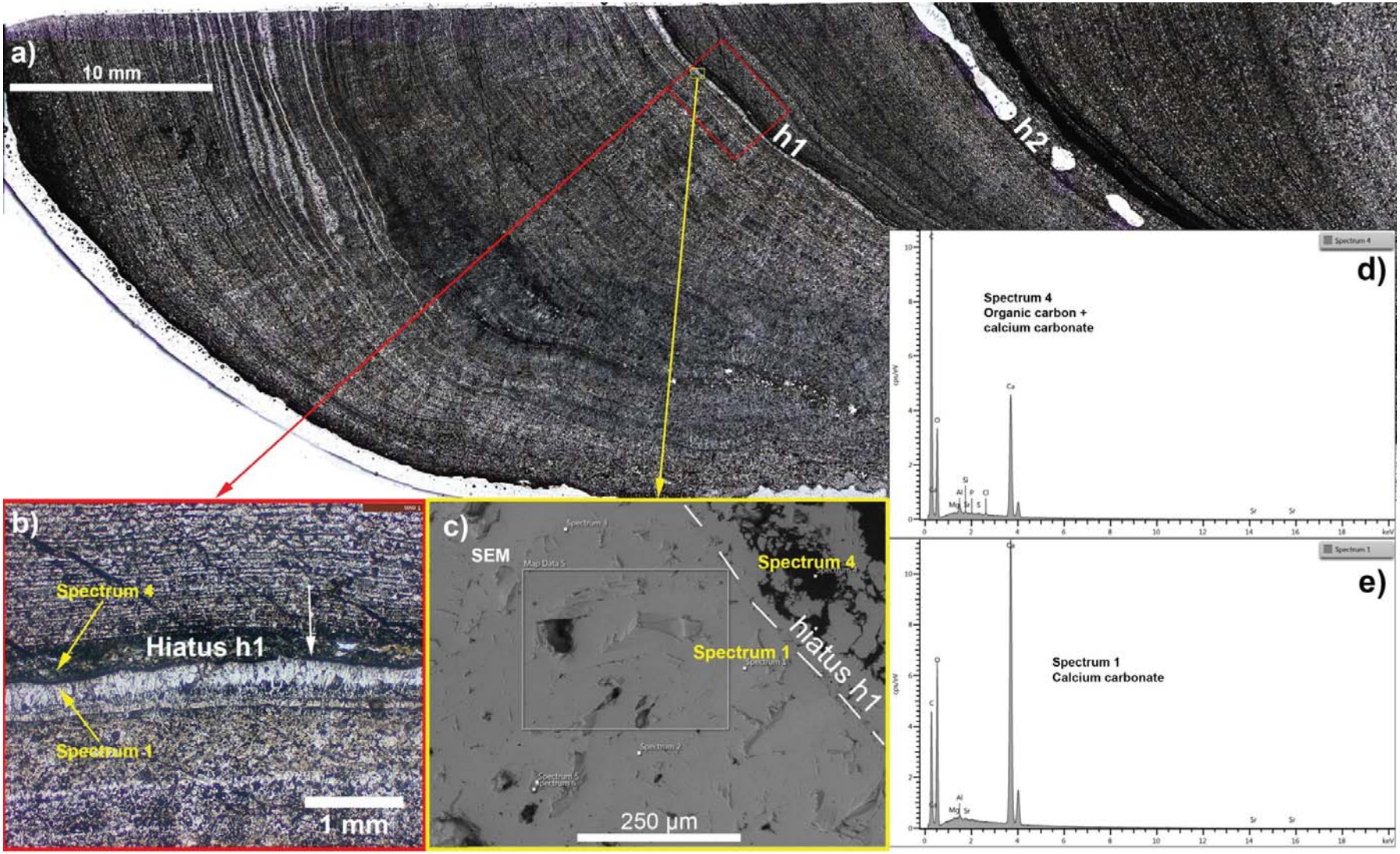
a)
10 mm
h1
h2
b)
Spectrum 4
Hiatus h1
Spectrum 1
1 mm
c)
SEM
Spectrum 4
Spectrum 1
hiatus h1
250 µm
d)
Spectrum 4
Organic carbon +
calcium carbonate
e)
Spectrum 1
Calcium carbonate

Fig. 4

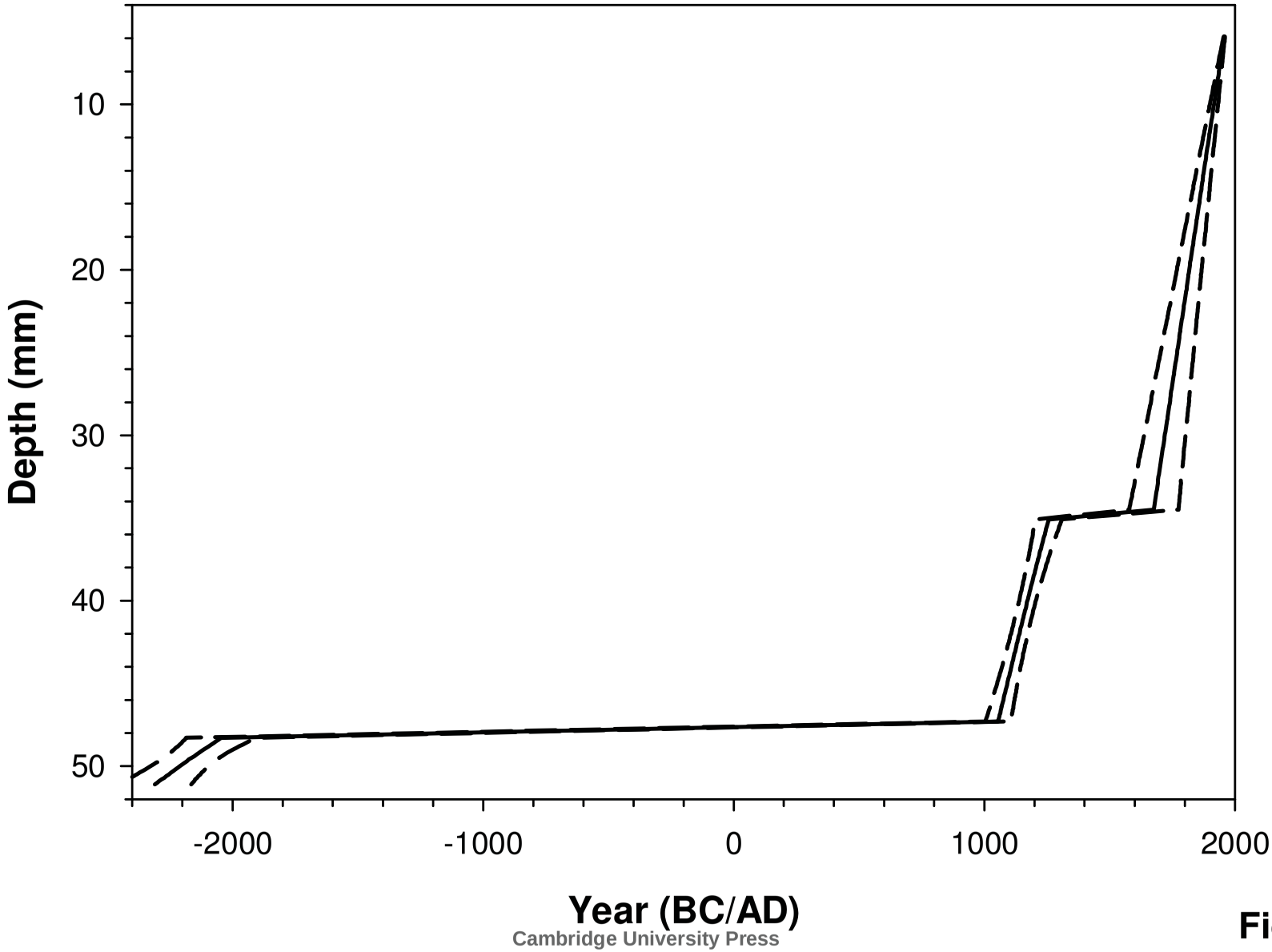

Fig. 5a

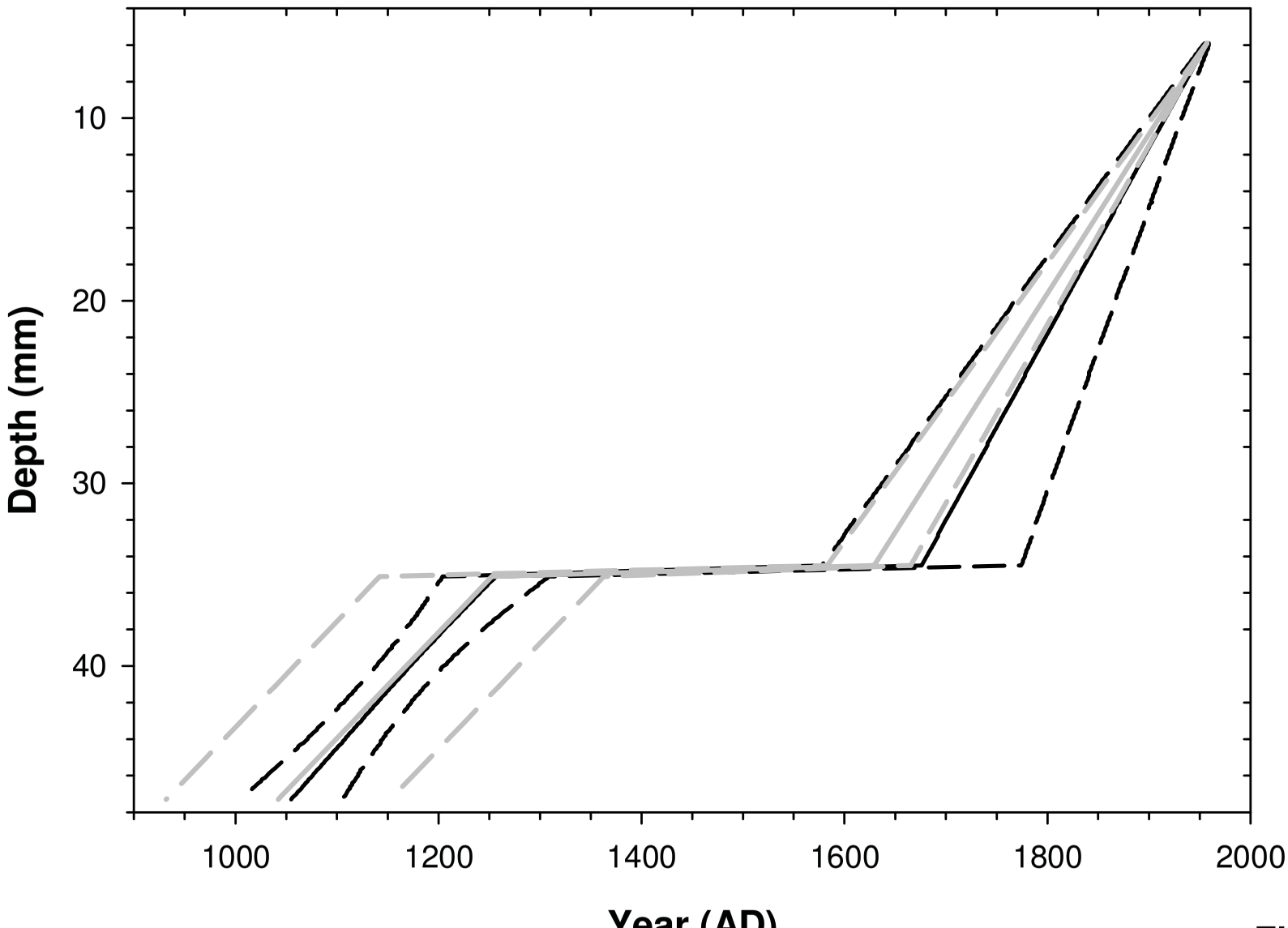

Fig. 5b

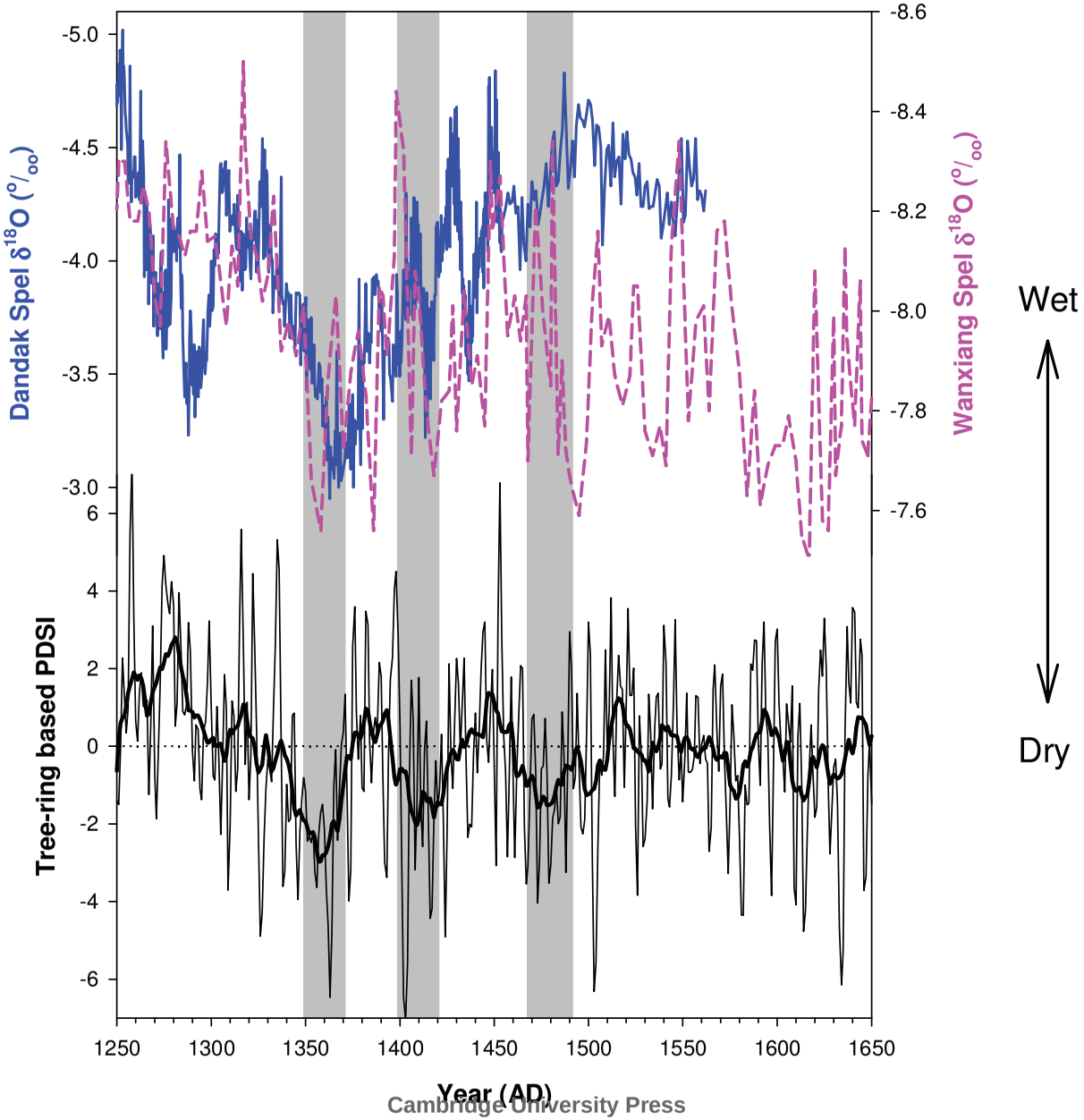

Fig. 6

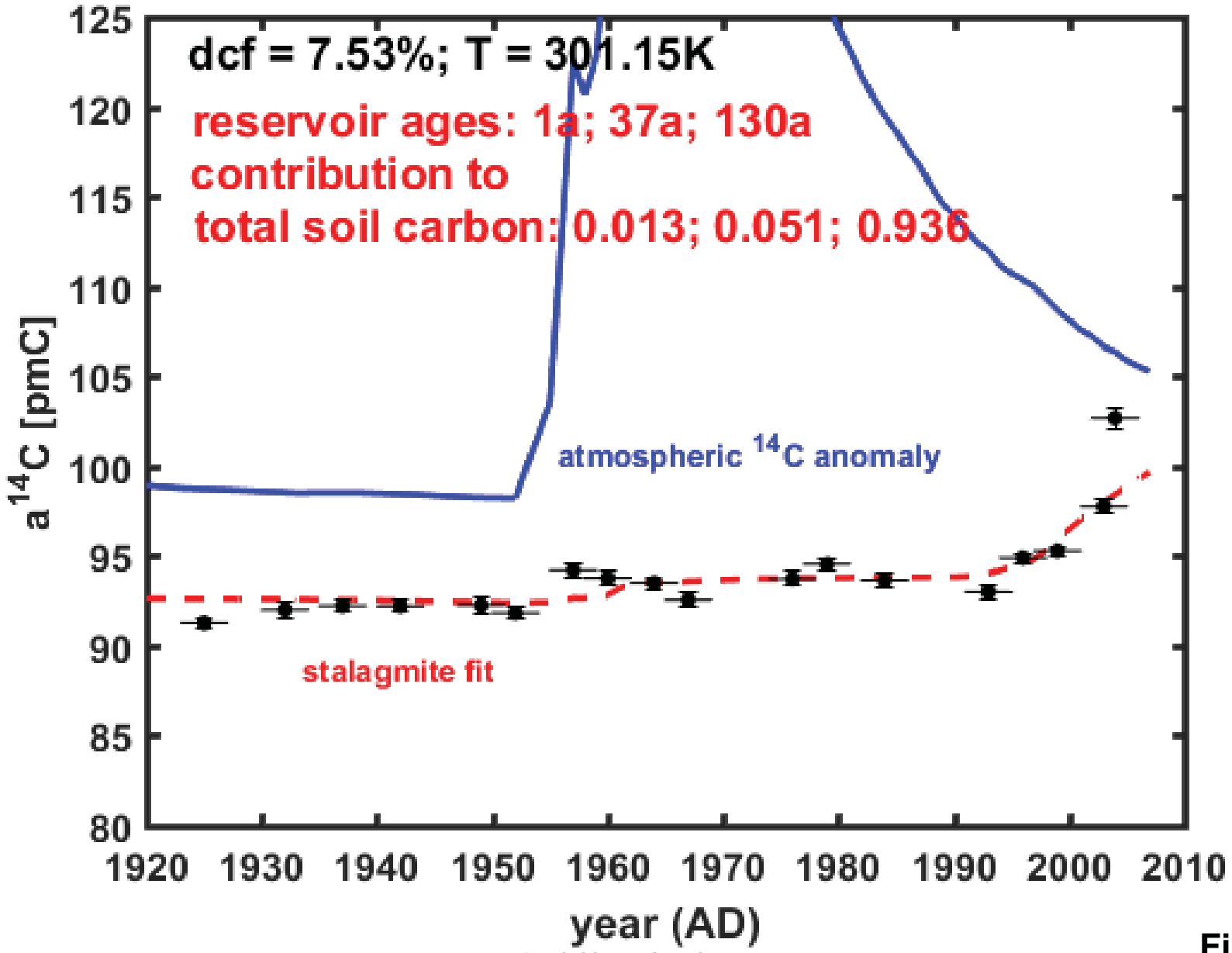

Fig. A1a

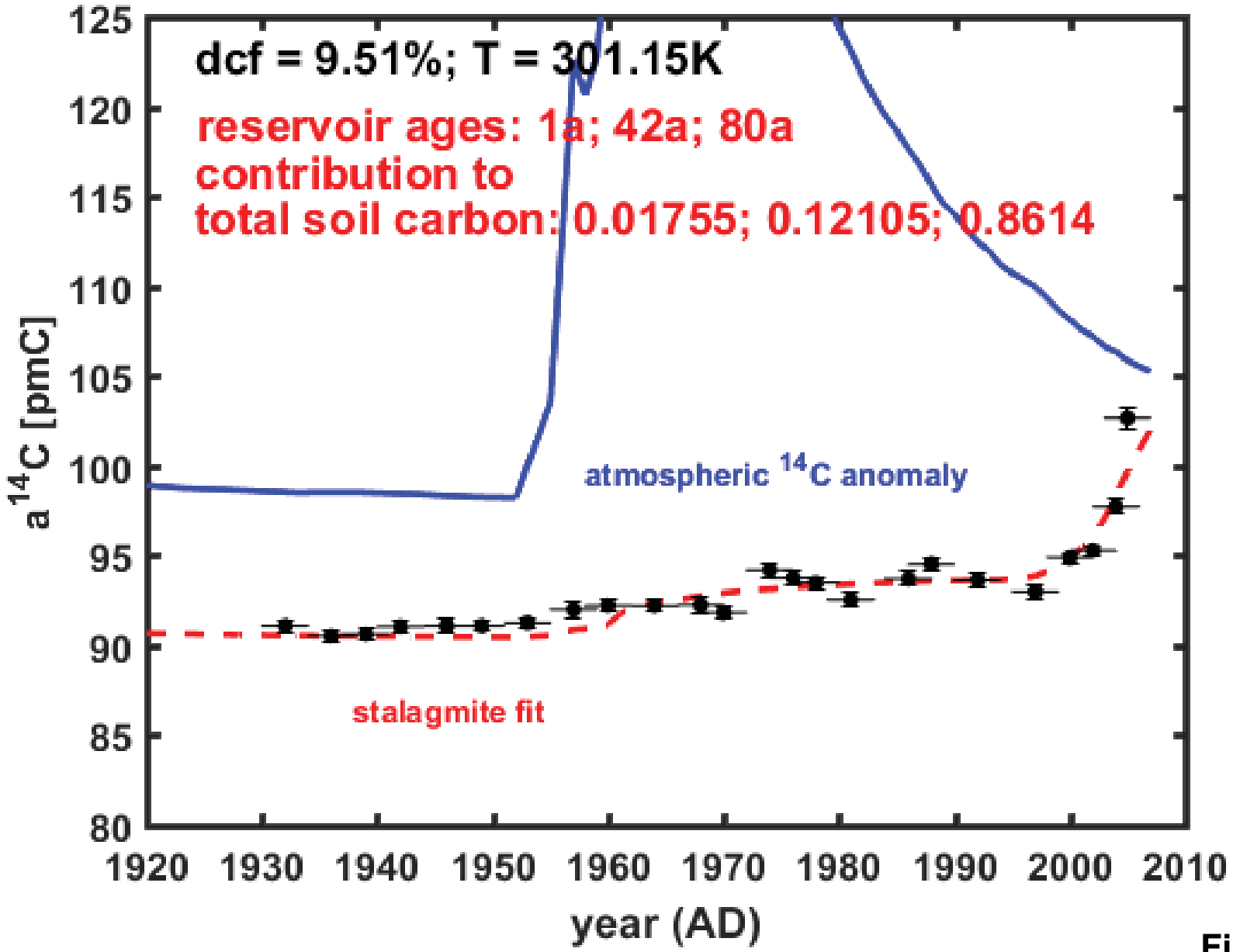

Fig. A1b